Nanoscale

ROYAL SOCIETY OF CHEMISTRY

PAPER

View Article Online
View Journal | View Issue

Cite this: *Nanoscale*, 2024, **16**, 19730

Metals in nanomotion: probing the role of extracellular vesicles in intercellular metal transfer

Qingyu Lei,[a] Thanh H. Phan,[b,g] Shiva Kamini Divakarla,[c] Bill Kalionis [d] and Wojciech Chrzanowski *[a,e,f]

Metals in living organisms and environments are essential for key biological functions such as enzymatic activity, and DNA and RNA synthesis. This means that disruption of metal ion homeostasis and exchange between cells can lead to diseases. EVs are believed to play an essential role in transporting metals between cells, but the mechanism of metal packaging and exchange remains to be elucidated. Here, we established the elemental composition of EVs at the nanoscale and single-vesicle level and showed that the metal content depends on the cell type and culture microenvironment. We also demonstrated that EVs participate in the exchange of metal elements between cells. Specifically, we used two classes of EVs derived from papaya fermented fluid (PaEVs), and decidual mesenchymal stem/stromal cells (DEVs). To show that EVs transfer metal elements to cells, we treated human osteoblast-like cells (MG63) and bone marrow mesenchymal stem cells (BMMSCs) with both classes of EVs. We found that both classes of EVs contained various metal elements, such as Ca, P, Mg, Fe, Na, Zn, and K, originating from their parent cells, but their relative concentrations did not mirror the ones found in the parent cells. Single-particle analysis of P, Ca, and Fe in DEVs and PaEVs revealed varying element masses. Assuming spherical geometry, the mean mass of P was converted to a mean size of 62 nm in DEVs and 24 nm in PaEVs, while the mean sizes of Ca and Fe in DEVs were smaller, converting to 20 nm and 30 nm respectively. When EVs interacted with BMMSCs and MG63, DEVs increased Ca, P, and Fe concentrations in BMMSCs and increased Fe concentration in MG63, while PaEVs increased Ca concentrations in BMMSCs and had no effect on MG63. The EV cargo, including proteins, nucleic acids, and lipids, differs from their origin in composition, and this variation extends to the element composition of EVs in our study. This fundamental understanding of EV-mediated metal exchange between cells could offer a new way of assessing EV functionality by measuring their elemental composition. Additionally, it will contribute novel insights into the mechanisms underlying EV production and their biological activity.

Received 9th July 2024,
Accepted 5th August 2024

DOI: 10.1039/d4nr02841d

rsc.li/nanoscale

Introduction

Metals and minerals play a pivotal role in maintaining cellular homeostasis, by supporting the health-related processes of living organisms. Currently, it is assumed that metals and minerals are exchanged between cells through secretomes, which are by-products produced by cells/microorganisms. However we know that intercellular exchange of the secretome is fundamental for the maintenance of cell function, and it is a primary mechanism of cell-to-cell communication. Here, we hypothesise that extracellular vesicles (EVs), which are key components of the secretome, contain and ferry metals and minerals between cells. We also hypothesize that the elemental composition of EVs is heterogeneous and depends not only on the cell, microorganism, and plant type but also on their microenvironments, which include extracellular matrix composition, architecture, and mechanobiological stressors.

A fundamental understanding of EV-mediated metal exchange is essential to advance the use of elemental composition as a biomarker of EV functionality and as biomarkers for diagnosing diseases, such as cancer. This new knowledge will shed light on the mechanisms of production of EVs and

[a]*Sydney Pharmacy School, Faculty of Medicine and Health, The University of Sydney, Camperdown 2006, Australia. E-mail: wojciech.chrzanowski@sydney.edu.au*
[b]*Centre for Immunology and Allergy Research, Westmead Institute for Medical Research, Westmead, NSW 2145, Australia*
[c]*BiomeCentric PTY LTD, 27 Expansion St, Molendinar 4214, QLD, Australia*
[d]*Department of Maternal-Fetal Medicine Pregnancy Research Centre, Royal Women's Hospital, and Department of Obstetrics, Gynaecology and Newborn Health, University of Melbourne, Parkville, VIC 3052, Australia*
[e]*Department of Laboratory Medicine, Division of Biomolecular and Cellular Medicine, Division of Clinical Immunology, Karolinska Institute, Sweden*
[f]*Division of Biomedical Engineering, Department of Materials Science and Engineering, Uppsala University, Sweden*
[g]*School of Medical Sciences, Faculty of Medicine and Health, The University of Sydney, Sydney NSW, Australia*

their biological functionality. This knowledge can be further used in EV manufacturing to develop bespoke EVs for different applications including functional food, pharmaceutical and veterinary formulations, as well as, for regenerative medicine and cosmeceutical applications.

Carbon (C), nitrogen (N), oxygen (O), and hydrogen (H) are essential elements to sustain living functions of cells and microorganisms. They are key components of biomolecules that form the primary building blocks of living organisms such as proteins, carbohydrates, lipids, and nucleic acids.[1] Furthermore, calcium (Ca), phosphorus (P), magnesium (Mg), sulfur (S), sodium (Na), and potassium (K), as well as, trace elements such as iron (Fe), zinc (Zn), iodine (I), selenium (Se), manganese (Mn), chromium (Cr), and copper (Cu), are necessary to control cell homeostasis and metabolism through binding with proteins to catalyze different biological reactions.[2] The elements including zinc (Zn), iron (Fe) and copper (Cu) also facilitate ion and oxygen transport, cellular respiration, DNA synthesis, and tissue formation.[3–5] Owing to their critical roles in the regulation of an organisms' bioactivities and in the interaction with biomolecules, metal elements play critical roles in cell function different applications including the production of medicines, biofuels and biomaterials.

To ensure optimal bioactivities of cells and microorganisms, the concentration of metals must be carefully controlled within appropriate ranges. Cells and microbes have sophisticated mechanisms to detect and control changes in the concentration of metal elements, which is known as metal homeostasis.[6] To regulate metal element concentration, most metals combine with varied membrane proteins, known as metal ion transporters, to pass through the plasma membrane, which facilitates the uptake and efflux of metal ions.[7] Different metals may rely on specific transporters or channels tailored for their transport. Some metals are transported across the cell membrane by specialized membrane proteins and integral membrane proteins.[8] Other metals are transported by endocytosis and exocytosis, which are active transport processes that utilize vesicles to facilitate the movement of molecules into and out of cells.[9]

Extracellular vesicles (EVs) are considered key mediators of intercellular communication that participate in the metal transport between cells. EVs comprise a heterogeneous population of cell-derived membranous vesicles, originating either from the endosomal compartment or the plasma membrane.[9,10] The release of EVs occurs in all three domains of cellular life (*i.e.*, Archaea, Bacteria and Eukarya), revealing a universal evolutionarily transitional mechanism for intercellular communication in both prokaryotes and eukaryotes.[11,12] EVs exchange biological cargoes, including nucleic acids (RNA and DNA), lipids and proteins between cells.[13] EVs act as signaling vehicles to maintain cellular homeostasis or to perform as a consequence of pathological developments.[10] Research on microbial-derived EVs has escalated over the last decade, due to the functional role of microbial-derived EVs in the transfer of cytoplasmic cargo, such as nucleic acids, virulence factors and cytoplasmic protein, which promote intra-kingdom and inter-kingdom interactions between bacteria and host.[14]

However, it is still unknown whether EVs inherit elements from their 'parent' cells and how uniformly they package elements into EVs of different sizes. Current research shows that cells package EVs with different cargos (*i.e.*, RNAs, proteins, lipids, metabolites) and decorate their surfaces with different surface protein markers. The composition of these cargoes and surface protein markers is dependent on the parent cell type and microenvironmental conditions such as stress and media composition. EVs contain metal elements but this has not been demonstrated in larger EV populations or at the single vesicle level.

Conventionally, the elemental composition of materials, including biological materials is performed by inductively coupled plasma mass spectrometry (ICP-MS). ICP-MS enables a precise measurement of elemental composition of liquid samples (resolution <ppb, *i.e.*, $\mu g\ L^{-1}$) with high-throughput samples and with high sensitivity.[15] ICP-MS is widely employed in clinical, biological, food, environmental, geological and industrial element analysis.[16] For example, ICP-MS detects the concentration of metal elements within the brain of mice and enabled the detection of age-related increases of copper, iron, and cobalt, which may be associated with the neurodegenerative disease.[17] Advanced ICP-MS instruments now provide detailed information of elemental composition and the size of nanoparticles by employing single nanoparticle inductively coupled plasma mass spectrometry (SP-ICP-MS). Li *et al.* showed that SP-ICP-MS determined the size distribution of gold nanoparticles and determined the assembly process of gold nanoparticle aggregates.[18] In summary, when ICP-MS and SC-ICP-MS are used together they are ideally placed to investigate the elemental composition of cells that produce EVs, the bulk elemental composition of large EV populations, and the elemental composition of individual EVs. Thus, by using these techniques it is possible to establish relationships between the compositions of (i) cells and EVs secreted by them, and (ii) EVs size and elemental composition as well as (iii) the ability of EVs to transfer elements to recipient cells.

Here we present the characterization of the elemental composition of EVs and cells, aiming to determine whether EVs possess a transport mechanism that facilitates the movement of elements into and out of cells. To achieve this, we used EVs extracted from papaya fermented fluid (PaEVs) and EVs isolated from a decidual mesenchymal stem/stromal cell line (DMSC23), called DEVs. These two EV sources were chosen because studies show that EVs derived from DMSC23 and papaya derivatives, such as papain, promote osteogenesis differentiation, which was associated with the likely presence of Ca and P in these EVs.[19,20] By detecting the concentration of metals such as Ca and P, osteogenesis can be tracked and quantified using ICPMS. Specifically, we measured (1) the elemental composition of different EV populations and their parent cells, (2) the elemental composition of individual EVs and their size distribution, and (3) the elemental composition of two types of recipient cells – human osteoblast-like cells (MG63) and bone marrow mesenchymal stem cells (BMMSCs) that were treated using both types of EVs. Here, we present a

novel method for characterizing EVs from an elemental perspective. This method not only facilitates the elucidation of the physical and chemical properties of EVs but also enables further investigation into the transport mechanisms of EVs within cells and their role in cellular communication.

Method

EV isolation and characterization

To isolate EVs we used: (1) the decidual mesenchymal stem/stromal cell line DMSC23, and (2) papaya fermented fluid (Rochway, Australia).

Cell culture

The DMSC23 cell line was derived from human term placenta as previously described.[21] DMSC23 were cultured in Mesencult™ MSC culture medium, containing Mesencult™ MSC Basal medium (Human) (STEMCELL Technologies), 10% stimulatory supplement in Basal medium (Human) (STEMCELL Technologies), 1% GlutaMAX™ (100× supplement, Life Technologies) and 1% pen/strep. To ensure optimal cellular viability, cells were passaged twice before being used for EV isolation.

The papaya fermented fluid (bio fermented papaya fruit + leaf, FPiP liquid) was obtained from Rochway and was kept refrigerated at 4 °C before EV isolation.

EV isolation

EVs were isolated using tangential flow filtration (TFF-EASY™, Lonza). Briefly, DMSC23 were cultured using Mesencult™ MSC culture medium before EV isolation. Once the confluency of DMSC23 reached 80%, cells were washed twice with Hanks' balanced salt solution [HBSS(−), Sigma-Aldrich] and maintained for 48 h in the EV isolation medium containing Mesencult™ MSC basal medium, 10% chemically defined medium for high density cell culture serum (CDM-HD, Sigma-Aldrich, USA) and 1% pen/strep. After 48 h, the EV-enriched isolation medium was collected into an RNase-free centrifuge tube and centrifuged for 5 min at 500*g*. The supernatant from the first centrifugation was transferred to another tube and centrifuged again for 10 min at 2000*g*. To remove cell debris, the supernatant from the final centrifugation was filtered using 0.45 μm filter (SFCA membrane, Corning®). EVs isolation, concentration and buffer exchange to phosphate-buffered saline (PBS) were performed using tangential flow filtration concentrator (TFF-EASY™, HansaBioMed/Lonza).

EVs from papaya fermented fluid (PaEVs) were isolated using TFF-EASY™ by the following steps. Papaya fermented fluid was collected into an RNase-free centrifuge tube and centrifuged for 5 min at 500*g*. The supernatant from the first centrifugation was transferred to another tube and centrifuged again for 10 min at 2000*g*. To remove cell debris, the supernatant from the final centrifugation was filtered using 0.45 μm filter (SFCA membrane, Corning®). EVs isolation. Concentration and buffer exchange to phosphate-buffered saline (PBS) were performed using TFF-EASY™.

In order to remove any potential residuals of the isolation media and PBS, DEVs and PaEVs were prepared using UltraPure™ Distilled Water (DNAse, RNAse, Free, Invitrogen, USA) and TFF-EASY™. The buffer exchange process of EVs was described in the manufacturer's protocol (HansaBioMed/Lonza) as previously introduced.[22] This step was essential to obtain high purity of DEVs and PaEVs samples without potential elemental contamination from the culture or isolation media.

EV characterization – EV quality control

To characterize DEVs and PaEVs, three EV quality attributes (QAs) were determined: size, size distribution, and concentration. QAs were measure using a nano flow analyzer (NanoFCM, Xiamen, China). The laser alignment and concentration calibration were performed using NanoFCM Quality Control Nanospheres (NanoFCM, Xiamen, China), and the size calibration was by NanoFCM Silica Nanospheres Cocktail #1 (NanoFCM, Xiamen, China). Prior to sample measurement, a PBS blank was used as control to remove the background. Samples were then loaded and size, size distribution and concentration were measured though scatter mode. All samples were collected for 120 s with total events collected ranged from 3000 to 6000 events.

Topographical measurement and analysis for EV size and shape were conducted using atomic force microscopy (AFM). EVs were diluted 1 : 100 in dH_2O then drop casted onto a mica disc, which was freshly cleaved using Scotch Tape. The droplet was left on the surface for 2 min, washed using dH_2O in triplicate, and then air-dried overnight. The prepared samples were scanned at 5 distinct points per sample and in triplicate, using AFM (Multimode 8, Bruker, USA) operating in Soft Tapping Mode using a silicon tip probe (SCOUT 350, NuNano, Bristol, UK): k = 42 N m^{-1}, 350 kHz. Analysis of data was undertaken using Mountains9 software (v. 9.2; DigitalSurf, Besançon, France).

Elemental analysis of EVs

To measure elemental composition of EVs, we used ICP-MS (PerkinElmer, Nexion 2000) with two different ICP-MS operating modes: (1) ICP-MS for bulk analysis, which provided a rapid and spontaneous multielement analysis of donors and EVs, and (2) single nanoparticle (SP) application, which determined size the distribution of specific elements in individual nanoparticles.

ICP-MS analysis for bulk analysis

To prepare the bulk-lysed EV sample, DEVs and PaEVs were lysed using 70% HNO_3 and further diluted 100× to 0.7% HNO_3 for elemental analysis. To determine the elemental composition of parental cells from which EVs were obtained, DMSC23 were counted and diluted at 10^6 mL^{-1} and 1 mL of cell suspension was pelleted using a centrifuge. Pelleted DMSC23 and 10 μL of papaya fermented fluid were lysed using 70% HNO_3 and further diluted 100× to 0.7% HNO_3 for elemental analysis. To investigate the elemental composition of biological samples while preventing spectral interference between

isotopes, we used the following isotopes: ^{43}Ca, ^{31}P, ^{57}Fe, ^{59}Co, ^{63}Cu, ^{66}Zn, ^{23}Na, ^{39}K, ^{24}Mg, ^{27}Al, ^{55}Mn and ^{62}Ni as target elements. Prior to sample measurement, elemental calibration of these elements was performed using distilled water as a blank and S4 multi-element mix (Choice Analytical, Australia) diluted 10×, 100×, 1000×, and 10 000×. Using a calibration curve obtained from the isotope-independent calibration, the elemental composition and concentration of bulk lysed EV samples and lysed donors were analysed and determined. All measurements were performed using a pump speed of 27 rpm.

SP-ICP-MS analysis for single EV analysis

The single-nanoparticle ICP-MS (SP-ICP-MS), was used with an operating mode developed to detect and count single nanoparticles, to measure the elemental composition and distribution in individual EVs.

Prior to measuring the EV samples, two types of standards were used: (i) gold particle standards with sizes of 50 nm and 100 nm to obtain accurate transport efficiency for counting signals, and (ii) dissolved calibration standards for calibration of the mass of the target element within each nanoparticle. The mass of the element within the nanoparticle was converted to size taking into consideration the spherical geometry of the element in the nanoparticle. For elemental standards, we selected ^{43}Ca, ^{31}P and ^{57}Fe as target elements and generated the calibration carve using distilled water as a blank and S4 multi-element mix (Choice Analytical, Australia), which was diluted into three dilutions of 10×, 100× and 1000×. Calibrating by gold standards and dissolved element standards of Ca, P and Fe, the mass/size of target elements, the mass/size distribution, counts of target element signals within DEVs and PaEVs were determined in the Syngistix™ Nano Application Module. All measurements were performed using a pump speed of 27 rpm, a sample uptake flow rate of 0.305 mL min^{-1} with a 50 μs dwell time, and a 60 s scan time.

Culture and elemental analysis of recipient cells

To determine whether elements can be transferred by EVs to recipient cells, we selected human osteosarcoma (MG63) and bone marrow mesenchymal stem cells (BMMSCs) as recipient cells. MG63 and BMMSCs are two types of cells that are commonly used to study cell mineralization and both DEVs and PaEVs showed the positive effects on mineralization in our previous study.[23]

Cell culture

BMMSCs were obtained from STEMCELL Technologies and cultured in Mesencult™ MSC culture medium, containing Mesencult™ MSC Basal medium (Human) (STEMCELL Technologies), 10% stimulatory supplement in Basal medium (Human) (STEMCELL Technologies), 1% GlutaMAX™ (100× supplement, Life Technologies) and 1% pen/strep. MG63 were cultured in DMEM culture medium, containing Dulbecco's modified Eagle's medium (DMEM medium-high glucose, Sigma-Aldrich), 10% foetal bovine serum (FBS, Bovogen, Australia) and 1% pen/strep. Hanks' balanced salt solution [HBSS(−), Sigma-Aldrich] was used for washing BMMSCs. Phosphate buffered saline (PBS, 10×, Sigma-Aldrich) was used for washing MG63. TrypLE™ Express (Gibco) was used as the dissociation reagent for adherent cells. All cell lines were maintained at 37 °C and 5% CO_2.

Elemental analysis of BMMSCs and MG63

To determine the capacity of EVs to modify the elemental composition of cells, both BMMSCs and MG63 were seeded in 96 well plates at 500 cells per well and maintained for 24 h. After 24 h, both cell types were treated with DEVs and PaEVs at two different concentrations: 10^2 and 10^4 EVs per cell. As a positive control, we used 100 nM and 10 nM of dexamethasone (Dex) for both types of cells. Dexamethasone is a steroid hormone that promotes extracellular matrix mineralization.[24] To induce pro-osteogenic differentiation with dexamethasone, the effective concentration range is within 10 nM to 100 nM for promoting osteogenic differentiation.[25] All the treatments were repeated every 7 days up to 21 days and cells were prepared at day 21. To prepare lysed cell samples for ICP-MS measurements, cells were washed 2 times with HEPES buffer, once with distilled water, and then lysed using 20 μL of 70% of HNO_3 in a 96 well plate. All samples were further diluted 50× for the elemental analysis. The measurements were performed using ICP-MS bulk analysis and three elements; ^{43}Ca, ^{31}P and ^{57}Fe, were measured.

Statistical analysis

Statistical analysis was carried out using GraphPad Prism software. Results were compared using one-way ANOVA with Turkey's multiple comparison test. Statistical significance was established at $p < 0.05$.

Results

Size and concentration of EVs

Topographical measurement and analysis of EV size and shape indicated that both DEVs and PaEVs exhibited heterogeneous sizes ranging from 40 to 200 nm. The analysis of EV morphology revealed predominantly uniform shapes of DEVs (Fig. 1A. Pink arrow), while most of the PaEVs were irregularly shaped (Fig. 1A. Yellow arrows), suggesting potential influences from extracellular matrix and aggregation on PaEVs (the presence of extracellular matrix corona).

The quantitative analysis of the size and size distribution EVs showed that the size of DEVs and PaEVs followed a near-Gaussian distribution with a size range of 40 to 200 nm (Fig. 1). DEVs had a mean size of 68.2 nm with a relatively large standard deviation (SD) of 20.8 nm, suggesting a diverse and spread-out size distribution of DEVs. However, PaEVs had a mean size of 55.4 nm with a standard deviation (SD) of 15.1 nm, indicating less size variation than DEVs. The analysis of EV concentration showed that the concentration of DEVs and PaEVs were 5.61×10^{10} EVs per ml and 2.55×10^9 EVs per ml, respectively (Fig. 1C).

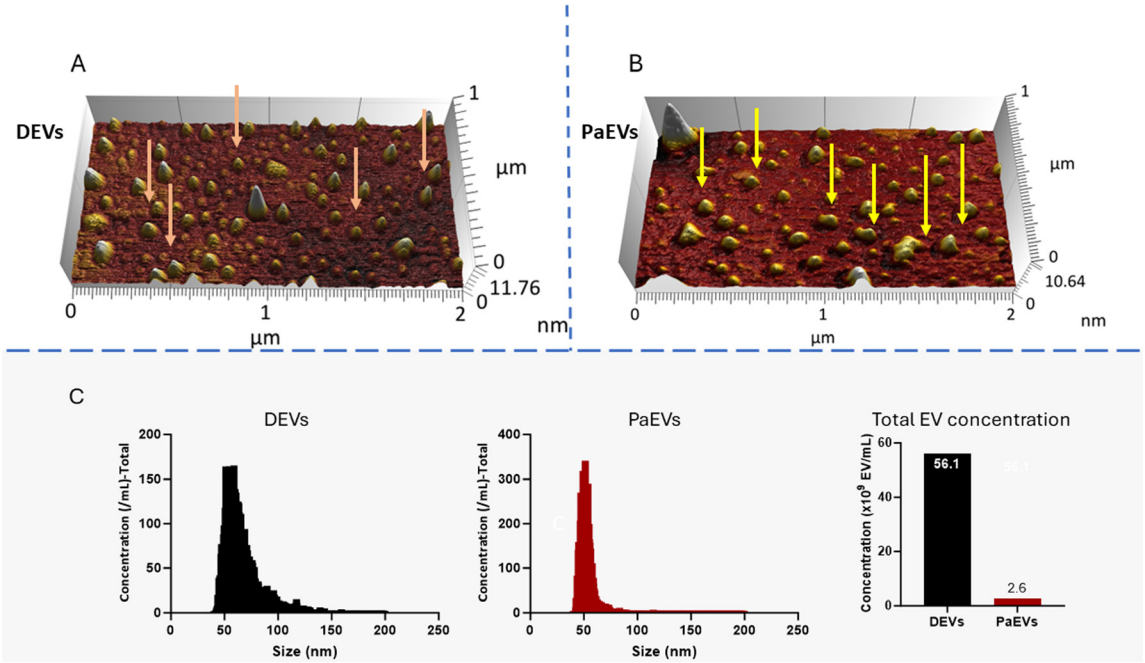

Fig. 1 Size and morphology of (A) DMSC23 EVs (DEVs) with symmetrical shapes pointed to by pink arrows and (B) papaya EVs (PaEVs) with asymmetric shapes pointed to by yellow arrows. (C) Size, size distribution and total concentration of DEVs and PaEVs.

Element composition between source of origin and isolated EVs

To establish a connection between the elemental composition of EVs and their source of origin, we conducted the elemental analysis on EV obtained from DMSC23 (DEVs) and DMSC23 cells, as well as on EVs isolated from papaya fermented fluid (PaEVs) and papaya fermented fluid (Fig. 2). The results revealed the presence of Ca, P, Mg, Fe, Na, Zn, and K in both DEVs and PaEVs. The same group of elements were also detected in DMSC23 and papaya fermented fluid. However, the relative concentrations of these elements were different between two types of EVs: DEVs and PaEVs. Additionally, differences of relative elemental concentrations were noted between EVs and their respective sources, such as between DMSCs and DEVs, but also between papaya fermented fluid and PaEVs.

DMSC23 contained Ca, P, Fe, Zn, Na, K, and Mg, where P, Na and K showed the highest concentrations at 937 µg L^{-1}, 642 µg L^{-1}, and 991 µg L^{-1}, respectively (Fig. 2A). Similarly, DEVs contained Ca, P, Mg, Fe, Na, Zn, and K, however the highest relative concentrations were observed for Ca (18 206 µg L^{-1}), P (35 358 µg L^{-1}) and Fe (73 885 µg L^{-1}) (Fig. 2C). Notably, Fe concentration was substantially higher in DEVs than in DMSC23, suggesting a potential role of DEV in maintaining calcium and iron homeostasis in parent cells and facilitating intracellular iron and calcium transfer.

The same group of metal elements, namely Ca, P, Fe, Zn, Na, K, and Mg, was found in the papaya fermented fluid. Amongst them Na, K and Mg showed the highest relative concentrations, which surpassed the detection limits. Additionally, the papaya fermented fluid contained Co, Al, Cu, Mn, and Ni (Fig. 2B). In contrast, PaEVs only contained Ca, P, Mg, Na, Zn, and K, and the highest relative concentrations were observed for P (1067 ppb) and Na (4847 ppb) (Fig. 2D). This indicates that PaEVs do not inherit all elements present in the source, and they are likely to facilitate the selective transfer of some elements, such as Na and P.

The analysis of the relative concentrations of elements and their contribution to the total amount of metal elements within one individual EVs revealed that the proportion of each element was different within DEVs and PaEVs (Fig. 2E). In DEVs, we found that Fe represented 51% of the total amount of all elements while P constituted 24%. Ca, Na and K represented 12%, 7% and 4% of total amount of elements respectively. The remaining elements such as Zn, Mg and Al, collectively comprised only 2%. In PaEVs, Na represented 72% of total amount of elements while P account for 16%. Mg and K comprised 6% and 4%, respectively, with the remaining elements, including Ca, Zn, and Al, collectively constituting 2%.

To enable an effective comparison of the elemental composition between single DEVs and PaEVs, we normalized the element concentration of EVs with the respective EV concentration obtained from NanoFCM (Fig. 2F). This allowed us to assess the relative quantities of each element at an averaged single EV level for both DEVs and PaEVs, with the results calculated in attograms (ag). The quantities of Ca, P, Na and Fe demonstrated the significant differences between DEVs and PaEVs. On average, DEVs contained 324 ag of Ca, 630 ag of P, 169 ag of Na and 1316 ag of Fe. In contrast, PaEVs had much lower amounts of Ca, Fe and P, with only 13 ag of Ca (24.4

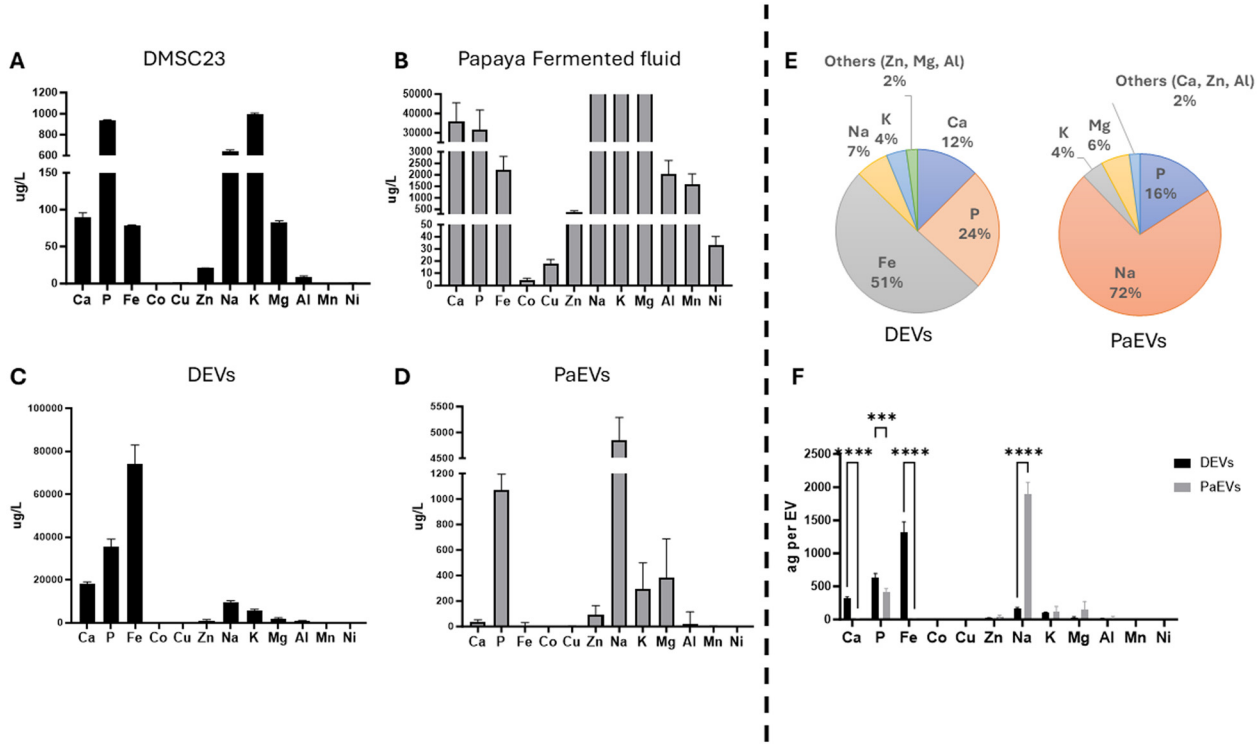

Fig. 2 Elemental composition of source of origin – (A) digested DMSC23, and (B) papaya fermented fluid and isolated EVs – (C) EV obtained from DMSC23 (DEVs) and (D) EVs isolated from papaya fermented fluid (PaEVs). Comparison of elemental compositions of single PaEV and single DEVs by averaging their elemental composition using concentrations obtained from NanoFCM, illustrated in both pie chart (E) and bar chart (F) (n = 3). Statistical significance was considered when the p-value was less than 0.05 (***: $p \leq 0.001$; ****: $p \leq 0.0001$; mean ± SD).

times lower than DEVs), 418 ag of P (1.5 times lower than DEVs), and 1 ag of Fe (1316 times lower than DEVs). However, PaEVs showed a higher amount of Na, with an amount of 1901 ag (11.2 times higher than DEVs).

Analysis of the element composition of individual EVs using SP-ICP-MS

To further investigate the correlation between the elemental composition and EV size, and determine how specific elements are packaged in individual EVs, we conducted SP-ICP-MS. This study provided us with key insights into the presence of specific elements in individual EVs. For this study, we analyzed concentrations of three major elements: phosphorus (P), calcium (Ca) and iron (Fe) (Fig. 3).

As SP-ICP-MS only can determine one type of element for each measurement, we assumed that EVs only contain one type of element in each measurement, for example, considering EVs as nanoparticles that contain only P, only Ca, or only Fe. After analyzing EVs by ICP-MS, pulse signals of P, Ca, and Fe were obtained separately. The intensity of pulse signals was converted to particle mass. Assuming EVs are spherical particles, the particle size of each element (P, Ca, and Fe) was calculated from the particle mass. Subsequentially, the resulting signals were converted into the size distribution for each element (P, Ca, and Fe) within EVs. The frequency was determined by counting the number of pulses/events. Each event corresponds to a signal from an individual particle. This correlation provides the information on the number of EVs that were detected and analyzed.

Phosphorus (P) is an essential element in the lipid membranes of EVs, hence it is likely that phosphorous will be distributed within the EV membrane. Hence, it was anticipated that the size of EVs measured based on the SC-ICP-MS would correlate with the actual size of EVs (measured using for example dynamic light scattering). Calcium (Ca) and iron (Fe), on the other hand, were likely packaged, or clustered inside EVs and associated with various cargo molecules, including proteins, nucleic acids, and other biomolecules, thus they may not reflect actual size of EVs.

We hypothesized that phosphorus (P) was distributed in the EV membrane, with the size of P closely aligning with the size of EVs. In contrast, calcium (Ca) and iron (Fe) were distributed within EV cargoes, and their presence in size could be attributed to the size of cargoes contained Ca and Fe.

Here, we determined the distribution of phosphorus (P) within DEVs and PaEVs and establish its correlation with EV size obtained from NanoFCM. The SP-ICP-MS results showed that DEVs had a strong phosphorous signal with the calculated particle size ranging from 14 to 152 nm (Fig. 3A). The average distribution of P in size within DEVs was 62.7 nm with a standard deviation (SD) of 16.13 nm. When comparing these results to the size obtained from NanoFCM, we found that the

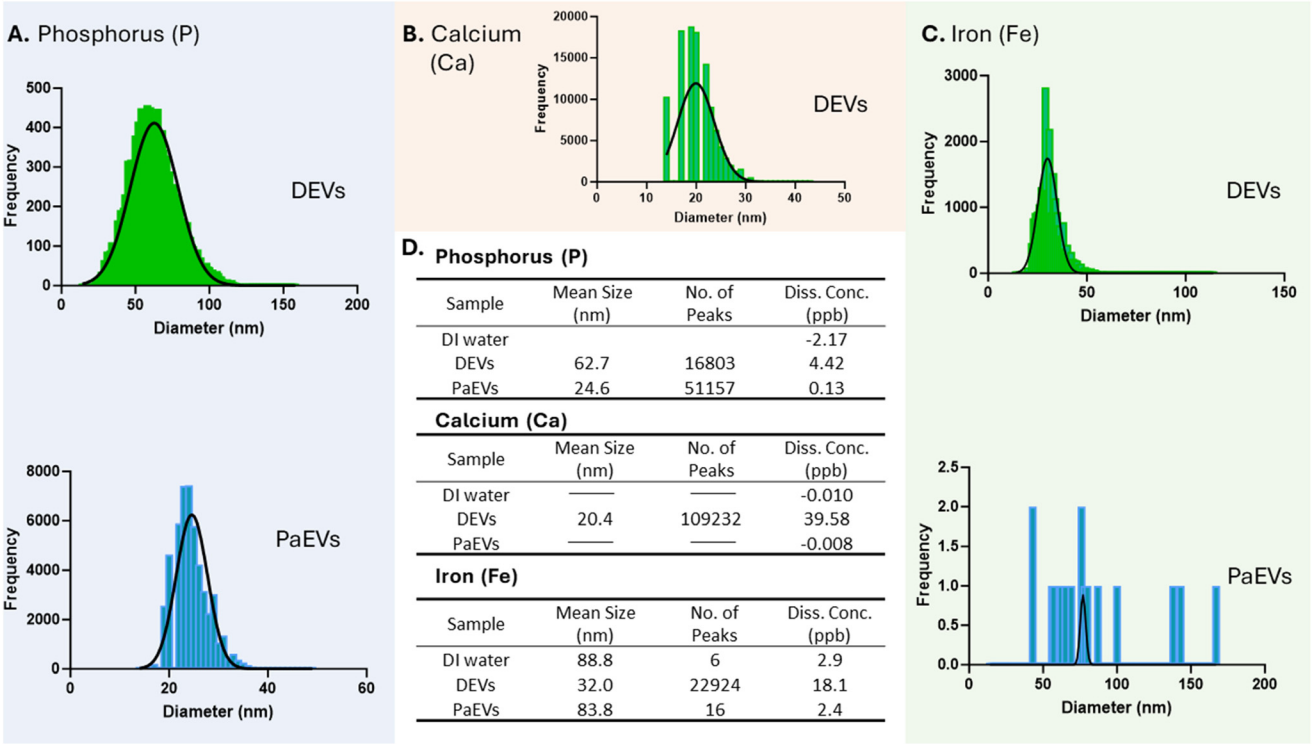

D.

Phosphorus (P)

Sample	Mean Size (nm)	No. of Peaks	Diss. Conc. (ppb)
DI water			-2.17
DEVs	62.7	16803	4.42
PaEVs	24.6	51157	0.13

Calcium (Ca)

Sample	Mean Size (nm)	No. of Peaks	Diss. Conc. (ppb)
DI water	——	——	-0.010
DEVs	20.4	109232	39.58
PaEVs	——	——	-0.008

Iron (Fe)

Sample	Mean Size (nm)	No. of Peaks	Diss. Conc. (ppb)
DI water	88.8	6	2.9
DEVs	32.0	22924	18.1
PaEVs	83.8	16	2.4

Fig. 3 (A) Size and size distribution of P within DEVs (n = 16 803 events) and PaEVs (n = 51 157 events), (B) size and size distribution of Ca within DEVs (n = 109 232 events) and (C) size and size distribution of Fe within DEVs (n = 22 924 events) and PaEVs (n = 16 events). (D) Quantitation of P Ca and Fe mean size, number of peaks and size and dissolved concentration of elements (diss. conc.).

average size of P within DEVs (62.7 nm) was close to the mean size of DEVs (68.2 nm). This similarity in size indicates a strong correlation between the size of P and the size of DEVs. On the other hand, for PaEVs, the SP-ICP-MS results showed a significant phosphorous signal, with the calculated particle size ranging from 14 to 50 nm. The average size of P within PaEVs was 24.6 with a standard deviation (SD) of 3.2 nm. When comparing these results to the size obtained from NanoFCM, we observed that the average size of P within PaEVs (24.6 nm) was smaller than the mean size of PaEVs (55.4 nm) indicating that the actual size of PaEVs could be smaller than the determined size.

Similarly, we determined the size of calcium (Ca) and iron (Fe) within DEVs and PaEVs respectively and established the correlation of their size with EV sizes obtained from NanoFCM. The SP-ICP-MS results showed strong signals of Ca and Fe within DEVs, with sizes ranging from 14 nm to 42 nm for Ca and 14 nm to 110 nm for Fe (Fig. 3B). The mean size of Ca was 20.4 nm with a SD of 3.7, while the mean size of Fe was 32.0 nm with a SD of 4.9. When compare these results to the size of DEVs, as well as the size of phosphorus (P) within DEVs, we observed that the size of Ca (20.4 nm) and the size of Fe (32.0 nm) were both smaller than the size of DEVs (68.2 nm) and size of P (62.7 nm). The smaller sizes of Ca and Fe suggested the possibility that these elements were encapsulated by DEVs, potentially being components within EV cargo. On other hand, no detectable signal for Ca was detected in PaEVs. 16 events of Fe were observed within PaEVs, with a mean size of 88 nm, similar to the mean size (d = 83 nm) and the number of Fe events detected in the background (water control, n = 6 events) (Fig. 3C & D). This indicated that Ca and Fe were not component presented within PaEVs.

Using SP-ICP-MS, we observed variations in event numbers when measuring different elements within the same analytical setup (Fig. 3D). When measuring phosphorus (P) within DEVs, we detected 16 803 P events (1000×), accounting for 0.1% of the EV concentration obtained by NanoFCM. In contrast, during the measurements of calcium (Ca) and iron (Fe) within DEVs, we detected 22 924 Fe events (2000×), accounting for 0.26% of the EV concentration, and 109 232 Ca events (400×), accounting for 0.25% of the EV concentration. If counting event number of P represents the EV number detected by ICP-MS, concentrations of Ca and Fe are 2.6 times and 2.5 times higher, respectively, than the concentration of P. This indicated that each EV may contains multiple Ca and Fe cargoes which were detected separately in SP-IC-MS.

Elemental result of lysed BMMSCs (MG63) treated with EVs

To investigate if EVs transfer calcium (Ca), phosphorus (P), and iron (Fe) to recipient cells, we treated BMMSCs and MG63 cells with both PaEVs and DEVs at two different concentrations and monitored the change in elemental composition within both type of cells.

The quantification of Ca within BMMSCs showed that when treated with a high concentration of PaEVs and DEVs (10^4 EVs per cell), the total Ca concentration increased significantly by 106% ($p \leq 0.05$) and 113% ($p \leq 0.01$), respectively, compared to non-treated cells. However, when BMMSCs were treated with PaEVs and DEVs at a low concentration (10^2 EVs per cell), there were no significant differences in Ca concentration compared to non-treated cells (Fig. 4A). Meanwhile, dexamethasone (DEX) had no effect on Ca concentration within BMMSCs whether treated at 100 nM and 10 nM.

The quantification of phosphorus (P) and iron (Fe) within BMMSCs showed that when treated with DEVs at a high concentration (10^4 EVs per cell), the total concentration of P increased by 48% ($p \leq 0.001$) and the total concentration of Fe increased by 46% ($p \leq 0.0001$). At a low concentration, DEVs had no effect on the P concentration but increased the concentration of Fe by 30%. PaEVs had no impact on P concentration but increased Fe concentration by 30% when treated with PaEVs at both high (10^4 EVs per cell) and low concentrations (10^2 EVs per cell) (Fig. 4B & C). The P concentration within BMMSCs showed no significant difference when they treated with dexamethasone (DEX) at concentrations of 100 nM and 10 nM. However, the concentrations of Fe increased by 40% (100 nM) and by 33% (10 nM) compared to non-treated cells.

The quantification of Ca and P within MG63 showed no significant difference between cells that were treated with PaEVs, DEVs, DEX and non-treated cells (Fig. 4D & E). However, when treated with DEVs at a high concentration (10^4 EVs per cell), the Fe concentration increased by 191% compared to non-treated cells, while at a low EV concentration (10^2 EVs per cell), the Fe concentration was no different with non-treated cells (Fig. 4F).

In summary, DEVs, when used at a high concentration, significantly increased the iron (Fe) concentration in both BMMSCs and MG63 cells, suggesting a potential role for DEVs in iron transport. Regarding calcium (Ca) and phosphorus (P) regulation, DEVs appeared to influence both Ca and P composition in BMMSCs but had no significant effect on MG63. Furthermore, PaEVs increased the Ca concentration in BMMSCs but had no impact on MG63 using both high and low EV concentrations.

Discussion

Donor cells define the elemental composition of EVs

Since EVs act as key signalling vehicles in normal cell homeostatic processes, they have potential as cell-free therapeutics to aid tissue repair for various conditions, including cardiac and bone.[26–28] However, cell homeostasis relies on metals and minerals to maintain physiological conditions and prevent pathological outcomes associated with metal ion imbalance.[29] Therefore, we hypothesize that EVs play a role in facilitating metal transport during cell-to-cell communi-

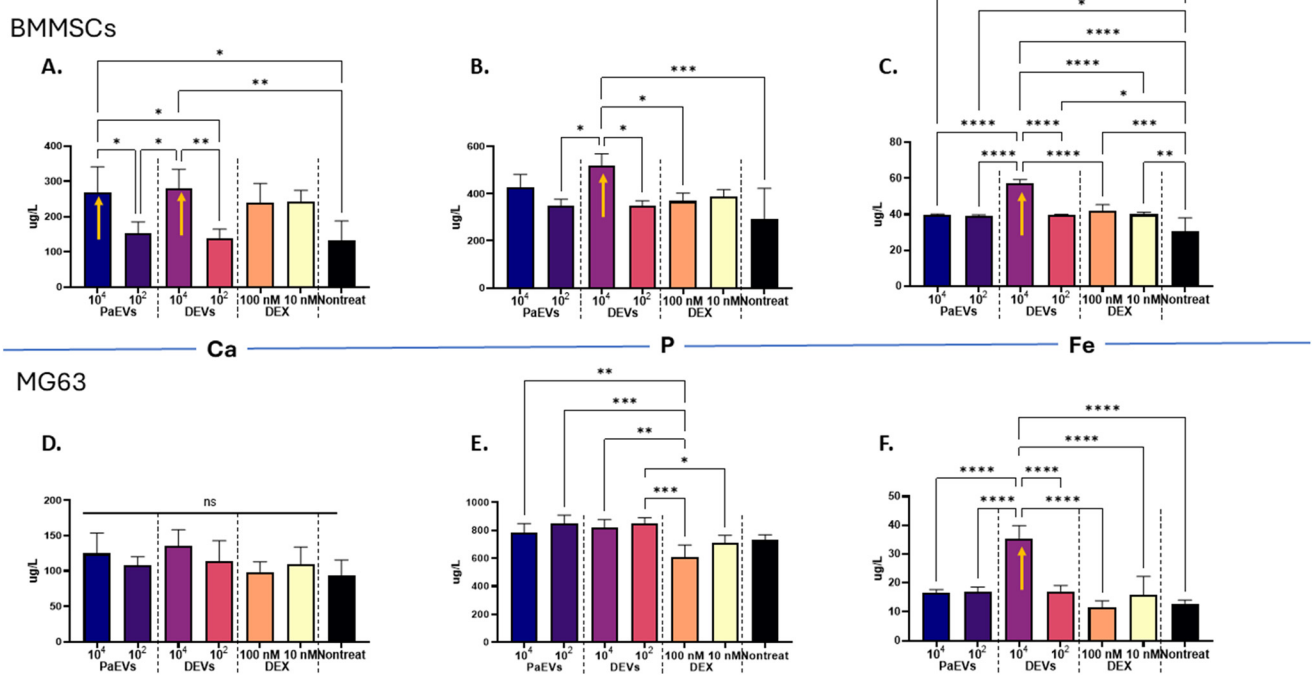

Fig. 4 Elemental composition of recipient cells BMMSCs and MG63 treated by PaEVs, DEVs and dexamethasone after 21 days. (A) Ca, (B) P and (C) Fe concentration within BMMSCs and (D) Ca, (E) P and (F) Fe concentration within MG63 (n = 3). The orange arrows indicated a significant increase compared to non-treated samples. A p-value less than 0.05 was considered statistically significant (ns: $p > 0.05$; *: $p \leq 0.05$; **: $p \leq 0.01$; ***: $p \leq 0.001$; ****: $p \leq 0.0001$; mean ± SD).

cation. Testing our hypothesis involved measuring the elemental composition of EVs from human stem cells and EVs produced during the fermentation of papaya. Both EV types were shown previously to have positive effects on processes that rely on metals and minerals homeostasis (*e.g.*, osteoinduction, osteoconduction).[23] Along with EVs we determined the elemental composition of the parent/donor cells of each EV type and showed that EVs inherit mineral elements from their parent/donor cells.

For EVs isolated from DMSCs (DEVs), Ca and P were detected in both DEVs and DMSC23. The presence of both elements within DEVs and DMSCs implies that EVs can transfer elements and modulate biological processes that rely on metal ions such as Ca and P. The transfer of these elements could support the basic functions of parent cells, including enhancing cell cycle progression, stimulating signal transduction, and regulating cell proliferation.[30,31] Considering the role of P in the synthesis of DNA and RNA and the formation of phospholipids and cellular membranes, the presence of P in DEVs can be attributed to the phospholipid membrane structure of EVs and their cargo content, which resembles that of their parent cells.[13,32] Additionally, we detected Fe in both DEVs and DMSCs and showed that EVs contained a higher amount of Fe than DMSCs, suggesting a role of EVs in iron homeostasis. Previous studies showed that the regulation of MSC-derived EVs in ferroptosis,[33,34] which our study attributes to the presence of Fe and its transfer through EVs.

The elemental composition of papaya fermentation-derived EVs (PaEVs) is influenced by elements from papaya and microorganisms like yeast and bacteria that can generate EVs.[35–37] Therefore, PaEVs isolated from papaya fermented fluid may contain elements such as K, Na, Mg, Ca, P and Zn derived from papaya fruit components (pulp, leaves, seeds),[38,39] and from microorganisms like yeast cells and bacteria, to support structural and functional roles in fermentation processes.[40,41] In our study, Ca, P, Fe, Zn, Na, K, and Mg were present in both papaya fermented fluid and PaEVs. Additionally, we found that PaEVs exhibit a high concentration of Na, suggesting a potential role of PaEVs in Na transfer and homeostasis. Previous studies reported that bacteria transport Na for harnessing energy and maintaining cellular homeostasis,[42] and our study implicates EVs in this transport. These discoveries expand the potential benefits of EV-based therapeutics, as the transfer of metals through EVs contributes to their multifunctionality and their ability to simultaneously regulate diverse biological processes.

While we revealed a close relationship between the contents of EVs and their parent cells, we made the novel discovery that EVs selectively pack certain elements, which highlights an aspect of composition unique to EVs. For example, DEVs contained significant amounts of Ca and Fe, with lower concentrations of Zn, Na, and K compared to the parent DMSCs. In contrast, PaEVs had high amounts of Na, while Mg, Co, Al, Cu, Mn, and Ni were only found in the fermented fluid and not in PaEVs. This selective packaging of elements observed in DEVs and PaEVs may be associated with EV cargo sorting mechanisms.[43] Additionally, by averaging element concentrations using EV concentrations, DEVs exhibited a higher concentration of P compared to PaEVs, which could be attributed to DEVs' larger size and greater membrane area dominated by phospholipids.[44,45]

However, the above elemental compositions of both DEVs and PaEVs were obtained from a bulk-dissolved method. This method, which measured dissolved EV samples, includes a significant amount of free ions[46] induced by environmental factors such as culture media, storage buffer (PBS), and degraded cell debris/EVs. This can lead to an overestimation of element concentrations within EVs. Furthermore, the bulk dissolution method cannot account for the heterogeneity in the biological cargo content of EVs,[47] leading to an expected heterogeneity in elemental content within EVs. Therefore, there is a need for a technique capable of distinguishing between free ions and those bound within EVs, while also verifying the heterogeneity of elements present within EVs. To overcome the challenges of distinguishing between free ions and those bound within EVs in bulk-dissolved methods, we used single particle-inductively coupled plasma-mass spectrometry (SP-ICP-MS).

Distribution of Ca, P, and Fe within EVs revealed by SP-ICP-MS

SP-ICP-MS distinguishes peaks generated by single-element clusters in nanoparticles from a steady baseline obtained from the same element solution using time-resolved analysis, thereby eliminating free ions from particle samples.[48] The single-element intensities from particles can be converted to the mass fraction of the element.[49] Assuming a spherical morphology of these elemental compounds, the mass fraction can further be converted to size fraction, allowing for the estimation of the size of elemental compounds within particles. Since the Ca, Fe and P were present in EVs at substantial and varied concentrations, these elements were selected for subsequent studies using SP-ICP-MS.

As phosphorus is a major component of the EV membrane, it can be assumed that its concentration correlates with the size of EVs. The estimated size of P within DEVs was ~60 nm, matching the size of DEVs measured by NanoFCM, indicating that the amount of P compounds in DEVs is associated with their actual size. For PaEVs, the converted size of P was ~25 nm, indicating lower P content and a smaller membrane area in PaEVs compared to DEVs. This finding aligns with the size measurements of PaEVs and DEVs, which showed that PaEVs are smaller in size compared to DEVs. However, this converted size of P was notably smaller than the size of PaEVs, which was ~55 nm as determined by NanoFCM. The larger PaEV size in measurements could result from PaEV aggregation, as indicated by their irregular shape in AFM images (Fig. 1B). Aggregation may result from the binding of extracellular biomolecules (*i.e.*, proteins, polysaccharides, and eDNA) that are co-secreted during bacterial EV production, to the EV surface.[50]

After converting the mass of Ca and Fe compounds within DEVs to a size, we found the size of Ca and Fe in DEVs were

~20 nm and ~30 nm, respectively, which were smaller than the measured DEV size (~60 nm), suggesting Ca and Fe may exist as small molecules, such as protein agglomerates, within or among DEVs. One potential explanation for this phenomenon is that Ca binds to Ca^{2+} effector proteins such as calmodulin or Ca^{2+}-sensing proteins like isocitrate dehydrogenase, while Fe in human cells is either stored as ferritin inside the cell or transferred to circulating transferrin *via* ferroportin on the plasma membrane.[51–53] Mattera *et al.* reported that EVs produced by mammalian cells carry Fe-associated proteins, including transferrin receptor 1 (TfR1), a carrier protein for transferrin, suggesting that EVs may facilitate the intracellular transport of apotransferrin.[54] Based on these studies, we speculate that the binding of Ca and Fe with proteins contributes to clusters of elements. Furthermore, the Ca and Fe peak signals were found predominantly in DEVs rather than PaEVs, suggesting the potential utility of elements as biomarkers to distinguish EVs derived from different cell sources.

Taken together, we propose that the size of elements is associated with their distribution within EVs. Specifically, the mass or estimated size of P in EVs corresponds to the membrane area of EVs, while the mass or estimated size of Ca and Fe in EVs corresponds to their respective cargo amounts (Fig. 5). Considering that Ca and Fe could be present within or among EVs, these elemental cargoes could distribute in two scenarios in Fig. 5: (1) Ca and Fe bind with membrane molecules and are distributed on the membrane of EVs, depicted in scenario 1; or (2) Ca and Fe bind with molecules and are encapsulated within EVs, as illustrated in scenario 2. For both scenarios, the signal of Ca and Fe can be measured by SP-ICP-MS due to the encapsulation of these elements within EVs. On the other hand, SP-ICP-MS estimates the number of element compounds loaded within EVs. Considering that phosphorus (P) is primarily distributed on the EV membrane, the number of P signals detected in SP-ICP-MS correlates with the number of EVs detected. The 2.6-fold higher number of Ca signals and 2.5-fold higher number of Fe signals compared to the number of P signals suggests that each EV may contain multiple Ca and/or Fe aggregates. Both discoveries extend potential applications of SP-ICP-MS in EV engineering for surface modification (Fig. 5, scenario 1) and cargo loading (Fig. 5, scenario 2), where selected elements can serve as markers to track the attachment or packaging of molecules within EVs at the single EV level.

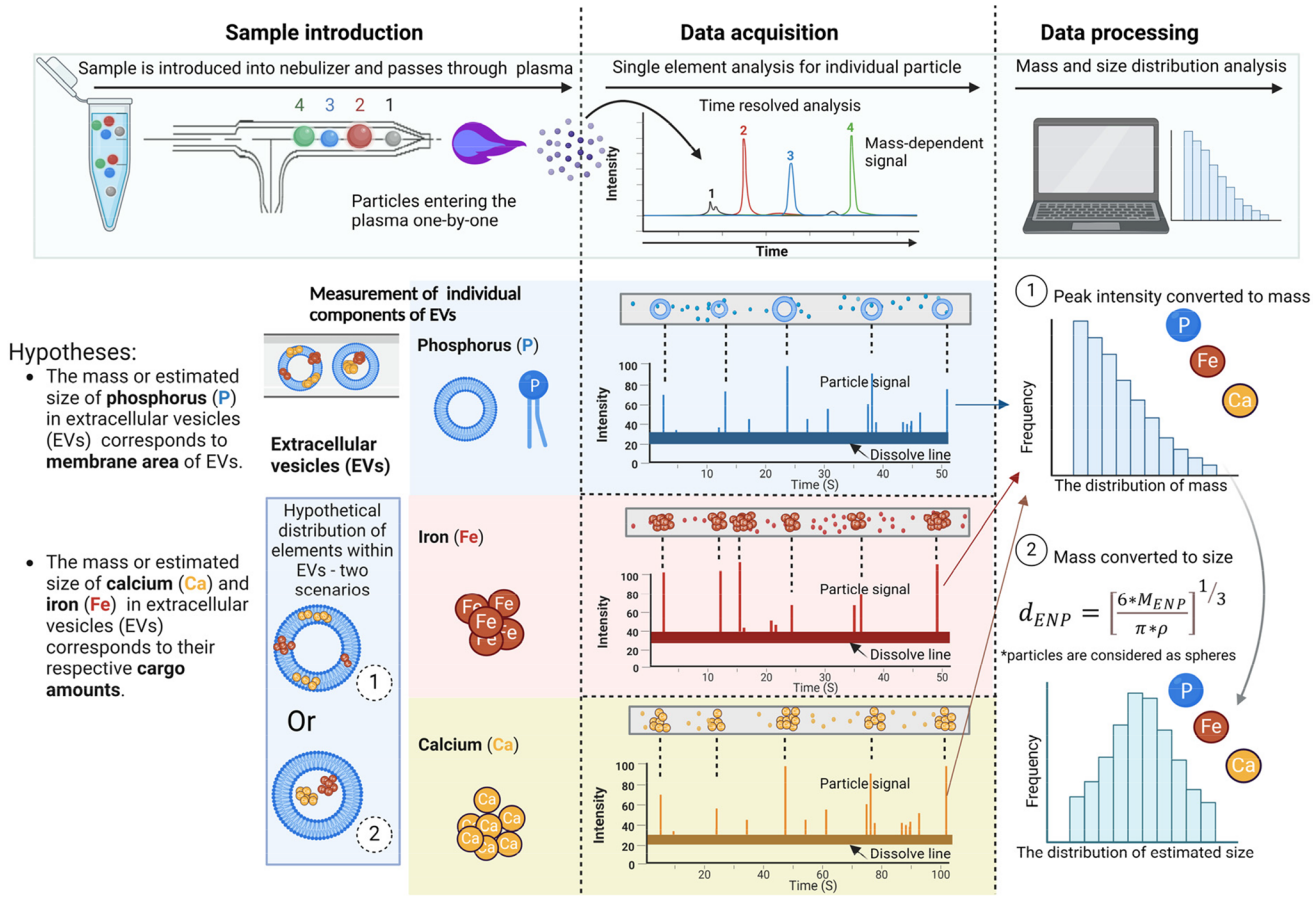

Fig. 5 Hypothetical composition of DEVs showing phosphorus (P) distribution on the membrane area and calcium (Ca) and iron (Fe) distribution within the cargo, with two hypothetical distribution scenarios. Size measurements of elements were conducted using single-element analysis with SP-ICP-MS and mass-to-size conventions.

However, not all detected Ca and Fe may originate from EVs; non-vesicular particles and protein aggregates with similar mass co-isolated with EVs could contribute to the peak signals during the detection.[55] The analysis of one isotope (m/z) at a time of SP-ICP-MS[49] limits its ability to comprehensively analyse complex EVs containing multiple elements. Therefore, conclusively attributing all detected elements to EVs and establishing direct relationships regarding their distribution within individual EVs is challenging. Furthermore, common interferences in ICP-MS, such as matrix effects caused by biological sample matrices (*e.g.*, EVs), can affect the analysis of the target analyte, leading to either underestimation or overestimation of the analyte amount, thereby hindering accurate mass quantification and size characterization.[56] Further development is needed to verify and accurately quantify multiple elements within EVs, including meticulous method validation such as matrix-matched calibration for enhanced reliability, advancing multi-element analysis capabilities, and improving instrument technology. These enhancements are crucial for overcoming current challenges and precisely characterizing the elemental composition of EVs.

Elemental transport by extracellular vesicles to recipient cells

Next, our study investigated the ability of EVs to transfer elemental cargo to recipient cells. When BMMSCs were treated with DEVs, the increase in intracellular concentrations of key elements like Ca, P and Fe post-internalization provided evidence of a direct transfer of these elements from the EVs to the recipient cells. Increased Ca and P within BMMSCs is linked to osteogenic differentiation,[57] thus the direct transfer of these elements by EVs provides new insight into the roles of EVs from stem cells in promoting bone regeneration through direct element transportation. The direct transfer of elements by EVs is a novel mechanism of EV action distinct from the well-established transfer of bioactive factors (*e.g.*, proteins, cytokines, lipids, miRNAs, and siRNAs) in the cargo of EVs to target cells.[58–60] Furthermore, we observed an increase of Fe within both BMMSCs and MG63 cells following treatment with DEVs, which provided evidence of Fe transfer by EVs to recipient cells. Thus, there is therapeutic potential for EVs in treating Fe deficiency diseases. We also detected an increase of Ca in BMMSCs treated with PaEVs, despite our observation that PaEVs contain a negligible amount of Ca. This increase of Ca is likely triggered by non-Ca bioactive factors carried by PaEVs, resulting in an indirect stimulation of the Ca synthesis pathway. Furthermore, we expect that MG63 cells have different mechanisms for regulating Ca and P levels, as shown by the lack of change in Ca and P levels in MG63 cells treated with DEVs, compared to BMMSCs treated with DEVs. This could be attributed to characteristic properties of MG63 cells, which are immortalized osteosarcoma cells. MG63 cells exhibit some properties of osteoblasts, resulting in different mineral compositions and baseline levels of osteocalcin, osteopontin, and osteonectin compared to BMMSCs.[61] Therefore, their response to stimuli such as Ca or P supplementation is expected to be different.

Collectively, these findings reveal the complex and multifaceted roles of EVs in cellular communication and regulation, demonstrating that EVs act not only as carriers of molecular and elemental cargo but also as modulators of cellular processes in recipient cells. EV-mediated cell communication plays a vital role in cell biology, regenerative medicine, and disease therapeutics. Consequently, the new understanding of EVs' role in maintaining mineral/metal homeostasis represents a significant advancement in EV research and has potential utility in biotechnology and therapeutic applications.

Conclusions

In conclusion, our study highlights the elemental composition of EVs from their parental cell origin to internalization by recipient cells. The presence of diverse metal elements, *i.e.*, Ca, P, Mg, Fe, Na, Zn, K, within PaEVs and DEVs is influenced by their cellular origin but exhibit unique characteristics in relative concentration and composition. Our methodology for single particle elemental analysis confirmed the presence of Ca, P, and Fe in EVs of varying amount, indicating not only diversity in size and biological content but also in the distribution of elements within individual EVs. Analysing the distribution of each element in size in relation to EV size further revealed insights into their location within the EV, either within the membrane or within the cargo. Furthermore, our findings underscore the pivotal role of EVs as carriers of elements such as Ca, P, and Fe, influencing the elemental composition of recipient cells. The exchange of elements by DEVs and PaEVs to MG63 and BMMSCs demonstrates that this exchange of element is EV-concentration dependent and recipient cell-type dependent. This fundamental understanding of EV-mediated metal exchange between cells could offer a new way of assessing EV functionality by measuring their elemental composition. Additionally, it will contribute novel insights into the mechanisms underlying EV production and their biological activity.

Author contributions

Q. L. and W. C. contributed to the conception and design of the study. T. H. P. and S. K. D. performed some experiments. Q. L. performed the statistical analysis. B. K. provided the experimental sources. Q. L. wrote the first draft of the manuscript. All authors contributed to the manuscript revision, read, and approved the submitted version.

Data availability

The authors declare that the data supporting the findings of this study are available within the paper, while raw data are stored in the University of Sydney repository. Should any raw data files be required they are available from the corresponding author upon reasonable request. Source data are provided in this paper.

Conflicts of interest

The authors declare that the research was conducted in the absence of any commercial or financial relationships that could be construed as a potential conflict of interest.

Acknowledgements

The authors acknowledge the facilities and the scientific and technical assistance of Sydney Mass Spectrometry, The University of Sydney, PerkinElmer. U.S. LLC and its affiliates. The authors acknowledge the figures created with BioRender.com. The authors would like to acknowledge the Australian Government for Research Training Program Scholarships (QL), Medical Advances Without Animals Trust MAWA (QL, THP and WC) and Wenner-Gren Foundations (WC).

References

1 S. Horowitz and R. C. Trievel, *J. Biol. Chem.*, 2012, **287**, 41576–41582.
2 M. A. Farag, B. Abib, Z. Qin, X. Ze and S. E. Ali, *Curr. Res. Food Sci.*, 2023, **6**, 100450.
3 K. Pantopoulos, S. K. Porwal, A. Tartakoff and L. Devireddy, *Biochemistry*, 2012, **51**, 5705–5724.
4 M. R. Bleackley and R. T. A. MacGillivray, *BioMetals*, 2011, **24**, 785–809.
5 L. M. Gaetke, H. S. Chow-Johnson and C. K. Chow, *Arch. Toxicol.*, 2014, **88**, 1929–1938.
6 A. J. Bird, *J. Nutr. Biochem.*, 2015, **26**, 1103–1115.
7 C. C. Philpott, *eLife*, 2014, **3**, e03997.
8 D. Wu, M. Saleem, T. He and G. He, *Membranes*, 2021, **11**, 984.
9 S. A. Bellingham, B. Guo and A. F. Hill, *Biol. Cell*, 2015, **107**, 389–418.
10 G. van Niel, G. D'Angelo and G. Raposo, *Nat. Rev. Mol. Cell Biol.*, 2018, **19**, 213–228.
11 S. Gill, R. Catchpole and P. Forterre, *FEMS Microbiol. Rev.*, 2019, **43**, 273–303.
12 M. Yáñez-Mó, P. R. M. Siljander, Z. Andreu, A. B. Zavec, F. E. Borràs, E. I. Buzas, K. Buzas, E. Casal, F. Cappello, J. Carvalho, E. Colás, A. Cordeiro-da Silva, S. Fais, J. M. Falcon-Perez, I. M. Ghobrial, B. Giebel, M. Gimona, M. Graner, I. Gursel, M. Gursel, N. H. H. Heegaard, A. Hendrix, P. Kierulf, K. Kokubun, M. Kosanovic, V. Kralj-Iglic, E.-M. Krämer-Albers, S. Laitinen, C. Lässer, T. Lener, E. Ligeti, A. Linē, G. Lipps, A. Llorente, J. Lötvall, M. Manček-Keber, A. Marcilla, M. Mittelbrunn, I. Nazarenko, E. N. M. Nolte-'t Hoen, T. A. Nyman, L. O'Driscoll, M. Olivan, C. Oliveira, É. Pállinger, H. A. Del Portillo, J. Reventós, M. Rigau, E. Rohde, M. Sammar, F. Sánchez-Madrid, N. Santarém, K. Schallmoser, M. S. Ostenfeld, W. Stoorvogel, R. Stukelj, S. G. Van der Grein, M. H. Vasconcelos, M. H. M. Wauben and O. De Wever, *J. Extracell. Vesicles*, 2015, **4**, 27066–27066.
13 C. Salomon, S. Das, U. Erdbrügger, R. Kalluri, S. K. Lim, J. M. Olefsky, G. E. Rice, S. Sahoo, W. A. Tao, P. Vader, Q. Wang and A. M. Weaver, *Endocr. Rev.*, 2022, **43**, 441–468.
14 A. Chronopoulos and R. Kalluri, *Oncogene*, 2020, **39**, 6951–6960.
15 S. C. Wilschefski and M. R. Baxter, *Clin. Biochem. Rev.*, 2019, **40**, 115–133.
16 E. Bulska and A. Ruszczyńska, *Phys. Sci. Rev.*, 2017, **2**, 20178002.
17 C. J. Maynard, R. Cappai, I. Volitakis, R. A. Cherny, A. R. White, K. Beyreuther, C. L. Masters, A. I. Bush and Q.-X. Li, *J. Biol. Chem.*, 2002, **277**, 44670–44676.
18 B.-R. Li, H. Tang, R.-Q. Yu and J.-H. Jiang, *Anal. Chem.*, 2020, **92**, 2379–2382.
19 M. Carnovali, G. Ramoni, G. Banfi and M. Mariotti, *Antioxidants*, 2021, **10**(12), 1987.
20 D. Wang, H. Cao, W. Hua, L. Gao, Y. Yuan, X. Zhou and Z. Zeng, *Membranese*, 2022, **12**(7), 716.
21 S. Q. Qin, G. D. Kusuma, B. Al-Sowayan, R. A. Pace, S. Isenmann, M. D. Pertile, S. Gronthos, M. H. Abumaree, S. P. Brennecke and B. Kalionis, *Placenta*, 2016, **39**, 134–146.
22 T. H. Phan, S. K. Divakarla, J. H. Yeo, Q. Lei, P. Tharkar, T. N. Pansani, K. G. Leslie, M. Tong, V. A. Coleman, Å. Jämting, M.-D. Du Plessis, E. J. New, B. Kalionis, P. Demokritou, H.-K. Woo, Y.-K. Cho and W. Chrzanowski, *Front. Bioeng. Biotechnol.*, 2021, **9**, 669537.
23 T. N. Pansani, T. H. Phan, Q. Lei, A. Kondyurin, B. Kalionis and W. Chrzanowski, *Nanomaterials*, 2021, **11**, 1445.
24 D. Fortunato, D. Mladenović, M. Criscuoli, F. Loria, K.-L. Veiman, D. Zocco, K. Koort and N. Zarovni, *Int. J. Mol. Sci.*, 2021, **22**(19), 1051.
25 M. Majrashi, A. Kotowska, D. Scurr, J. M. Hicks, A. Ghaemmaghami and J. Yang, *ACS Appl. Mater. Interfaces*, 2023, **15**, 56623–56638.
26 Y. Zhang, Y. Liu, H. Liu and W. H. Tang, *Cell Biosci.*, 2019, **9**, 19–19.
27 X. Zhang, Y. Wu, Q. Cheng, L. Bai, S. Huang and J. Gao, *Front. Cell Dev. Biol.*, 2022, **10**, 875376.
28 F. Fang, J. Yang, J. Wang, T. Li, E. Wang, D. Zhang, X. Liu and C. Zhou, *Bone Res.*, 2024, **12**, 4.
29 B. Michalke and V. Venkataramani, *Int. J. Mol. Sci.*, 2023, **24**, 4889.
30 N. Ahamad, Y. Sun and B. B. Singh, *Stem Cell Res.*, 2021, **56**, 102560.
31 S. Kim, J. Piao, Y. Son and H. S. Hong, *Biochem. Biophys. Res. Commun.*, 2017, **485**, 131–137.
32 M. P. Zaborowski, L. Balaj, X. O. Breakefield and C. P. Lai, *Bioscience*, 2015, **65**, 783–797.
33 Z. Liao, B. Tong, Z. Ou, J. Wei, M. Lei and C. Yang, *Traffic*, 2023, **24**, 384–396.
34 F. Lin, W. Chen, J. Zhou, J. Zhu, Q. Yao, B. Feng, X. Feng, X. Shi, Q. Pan, J. Yu, L. Li and H. Cao, *Cell Death Dis.*, 2022, **13**, 271.

35 M. Logozzi, R. Di Raimo, D. Mizzoni and S. Fais, *Int. J. Mol. Sci.*, 2021, **22**(15), 8170.
36 D. L. Oliveira, E. S. Nakayasu, L. S. Joffe, A. J. Guimarães, T. J. Sobreira, J. D. Nosanchuk, R. J. Cordero, S. Frases, A. Casadevall, I. C. Almeida, L. Nimrichter and M. L. Rodrigues, *PLoS One*, 2010, **5**, e11113.
37 M. Li, K. Lee, M. Hsu, G. Nau, E. Mylonakis and B. Ramratnam, *BMC Microbiol.*, 2017, **17**, 66.
38 A. Hardisson, C. Rubio, A. Baez, M. Martin and R. Alvarez, *Eur. Food Res. Technol.*, 2001, **212**, 175–181.
39 L. F. Santana, A. C. Inada, B. L. S. d Espirito Santo, W. F. O. Filiú, A. Pott, F. M. Alves, R. C. A. Guimarães, K. C. Freitas and P. A. Hiane, *Nutrients*, 2019, **11**(7), 1608.
40 G. Walker, *Adv. Appl. Microbiol.*, 2004, **54**, 197–229.
41 M. Samtiya, R. Aluko, A. Puniya and T. Dhewa, *Fermentation*, 2021, **7**, 63.
42 M. Ito and B. Barquera, in *Binding, Transport and Storage of Metal Ions in Biological Cells*, ed. W. Maret and A. Wedd, The Royal Society of Chemistry, 2014, DOI: **10.1039/9781849739979-00006**.
43 Y. J. Lee, K. J. Shin and Y. C. Chae, *Exp. Mol. Med.*, 2024, **56**, 877–889.
44 K. Kritmetapak and R. Kumar, *Calcif. Tissue Int.*, 2021, **108**, 16–31.
45 M. Record, S. Silvente-Poirot, M. Poirot and M. O. Wakelam, *J. Lipid Res.*, 2018, **59**, 1316–1324.
46 S. Wilbur, M. Yamanaka and S. Sannac, Characterization of nanoparticles in aqueous samples by ICP-MS White paper, 2015.
47 J. Wang, A. Wuethrich, R. J. Lobb, F. Antaw, A. A. I. Sina, R. E. Lane, Q. Zhou, C. Zieschank, C. Bell, V. F. Bonazzi, L. G. Aoude, S. Everitt, B. Yeo, A. P. Barbour, A. Möller and M. Trau, *ACS Sens.*, 2021, **6**, 3182–3194.
48 F. Laborda, E. Bolea and J. Jiménez-Lamana, *Anal. Chem.*, 2014, **86**, 2270–2278.
49 D. Mozhayeva and C. Engelhard, *J. Anal. At. Spectrom.*, 2020, **35**, 1740–1783.
50 M. Potter, C. Hanson, A. J. Anderson, E. Vargis and D. W. Britt, *Sci. Rep.*, 2020, **10**, 21289.
51 R. Bagur and G. Hajnóczky, *Mol. Cell*, 2017, **66**, 780–788.
52 E. Carafoli and J. Krebs, *J. Biol. Chem.*, 2016, **291**, 20849–20857.
53 C. Camaschella, A. Nai and L. Silvestri, *Haematologica*, 2020, **105**, 260–272.
54 V. S. Mattera, P. P. Gerber, R. Glisoni, M. Ostrowski, S. V. Verstraeten, J. M. Pasquini and J. D. Correale, *J. Neurochem.*, 2020, **155**, 327–338.
55 J. Maia, S. Batista, N. Couto, A. C. Gregório, C. Bodo, J. Elzanowska, M. C. Strano Moraes and B. Costa-Silva, *Front. Cell Dev. Biol.*, 2020, **8**, 593750.
56 Y. Huang, J. T. Lum and K. S. Leung, *J. Anal. At. Spectrom.*, 2020, **35**, 2148–2155.
57 F. Viti, M. Landini, A. Mezzelani, L. Petecchia, L. Milanesi and S. Scaglione, *PLoS One*, 2016, **11**, e0148173.
58 M. Somiya, *J. Cell Commun. Signaling*, 2020, **14**, 135–146.
59 N. Al-Sharabi, S. Mohamed-Ahmed, S. Shanbhag, C. Kampleitner, R. Elnour, S. Yamada, N. Rana, E. Birkeland, S. Tangl, R. Gruber and K. Mustafa, *Stem Cell Res. Ther.*, 2024, **15**, 33.
60 Z.-X. Wang, X. Lin, J. Cao, Y.-W. Liu, Z.-W. Luo, S.-S. Rao, Q. Wang, Y.-Y. Wang, C.-Y. Chen, G.-Q. Zhu, F.-X.-Z. Li, Y.-J. Tan, Y. Hu, H. Yin, Y.-Y. Li, Z.-H. He, Z.-Z. Liu, L.-Q. Yuan, Y. Zhou, Z.-G. Wang and H. Xie, *J. Nanobiotechnol.*, 2024, **22**, 208.
61 R. Florencio-Silva, G. R. Sasso, E. Sasso-Cerri, M. J. Simões and P. S. Cerri, *BioMed Res. Int.*, 2015, **2015**, 421746.